National Aeronautics and Space Administration

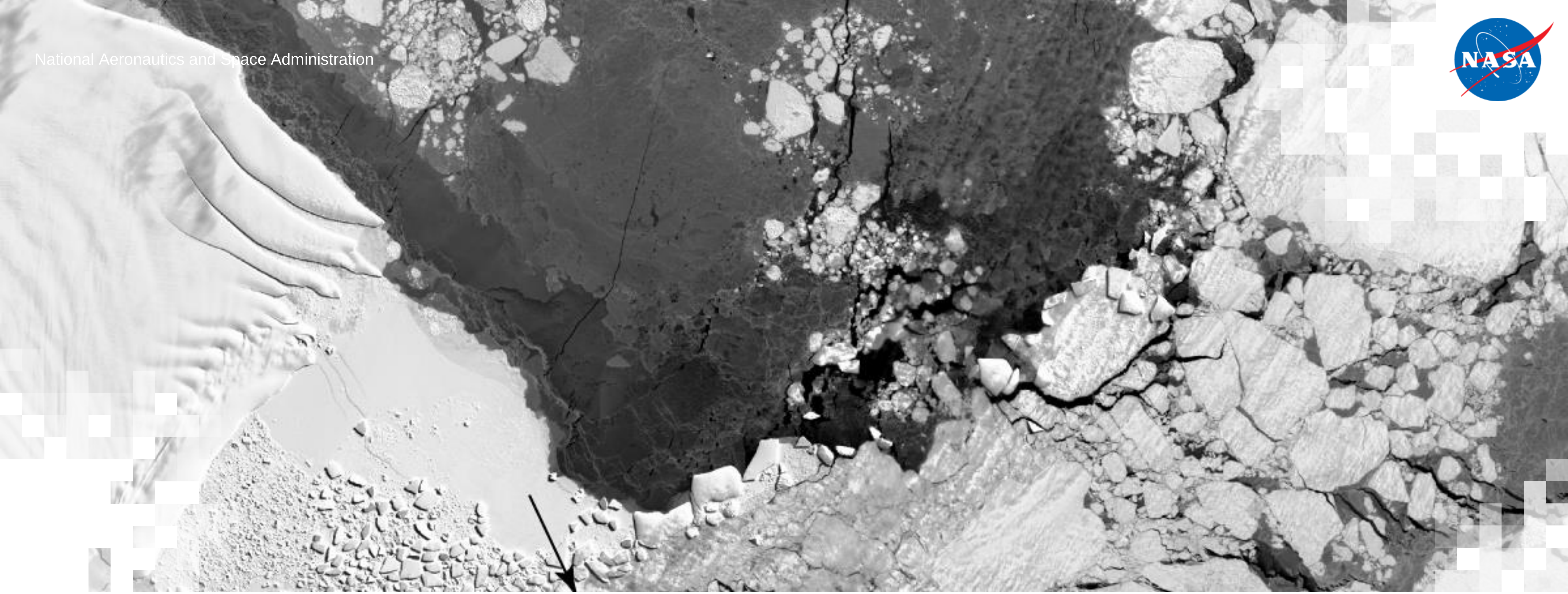

SAR for Detecting and Monitoring Floods, Sea Ice, and Subsidence from Groundwater Extraction

Session 2: Measuring Surface Subsidence due to Groundwater Extraction with InSAR

Eric Jameson Fielding and Zhen Liu (Jet Propulsion Laboratory, California Institute of Technology)

October 31, 2023

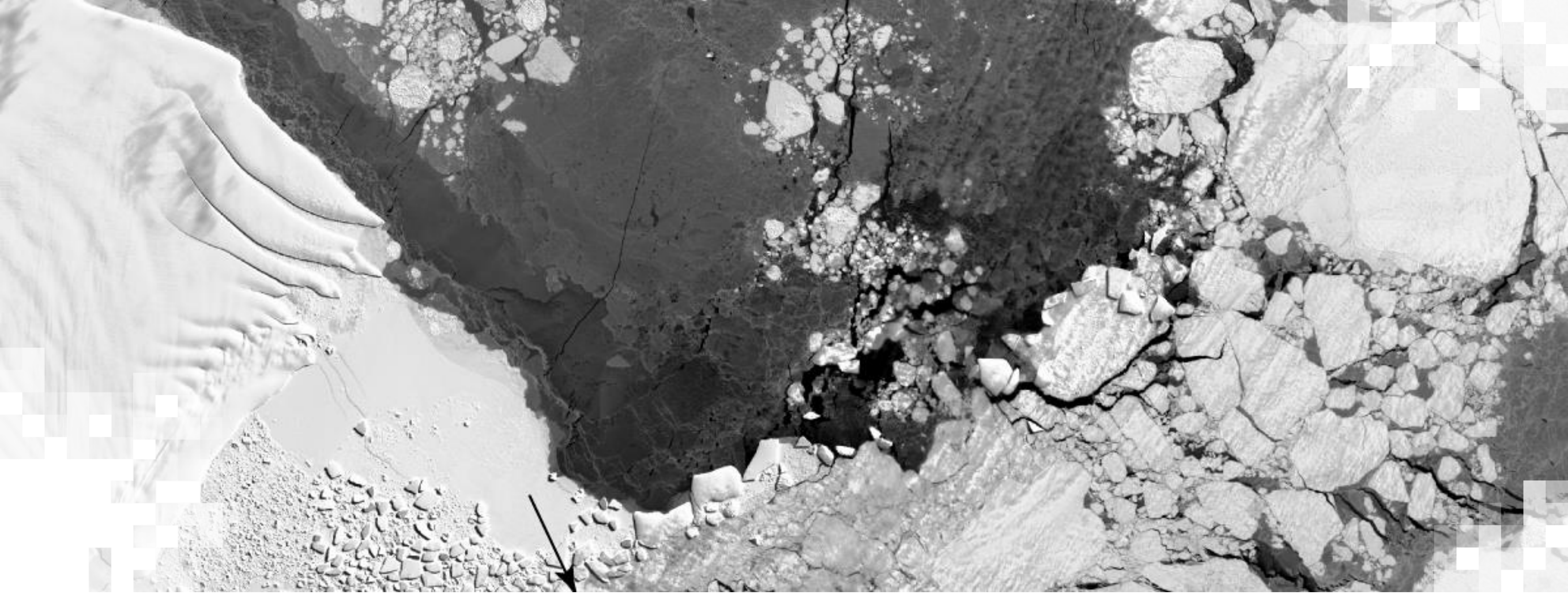

SAR for Detecting and Monitoring Floods, Sea Ice, and Subsidence from Groundwater Extraction

Overview

Sea Ice, Floods and Groundwater Extraction can be Seen from Space

- The objective of this webinar series is for participants to learn how to use SAR to detect and address potential disasters related to sea ice, floods and groundwater extraction.

- These sort of events can have a large impact on human lives, infrastructure and the economy.

- SAR can be critical in informing on-the-ground efforts on disaster mitigation efforts and resilience.

Training Learning Objectives

By the end of this webinar series, participants will be able to:

- Generate subsidence maps due to groundwater extraction to inform risk and resource management.
- Detect and monitor sea ice to identify potential risks to shipping and coastal erosion.
- Detect and monitor floods in order to more closely monitor increase/decrease of flood waters and better inform disaster response and management.

Training Outline

Session 1

Detecting and Monitoring Sea Ice with SAR

Tue. Oct. 24, 2023

11:00-13:00 EDT (UTC-4)

Session 2

Measuring Surface Subsidence due to Groundwater Extraction with InSAR

Tue. Oct. 31, 2023

11:00-13:00 EDT (UTC-4)

Session 3

Detecting and Monitoring Floods with SAR

Wed. Nov. 1, 2023

11:00-13:00 EDT (UTC-4)

Homework

Opens Nov. 1– Due Nov. 17 – Posted on Training Webpage

A certificate of completion will be awarded to those who attend all live sessions and complete the homework assignment(s) before the given due date.

How to Ask Questions

- Please put your questions in the Questions box. It is located at the bottom right under the three points. We will address them at the end of the webinar.
- Feel free to enter your questions as we go. We will try to get to all of the questions during the Q&A session after the webinar.
- The remainder of the questions will be answered in the Q&A document, which will be posted to the training website about a week after the training.

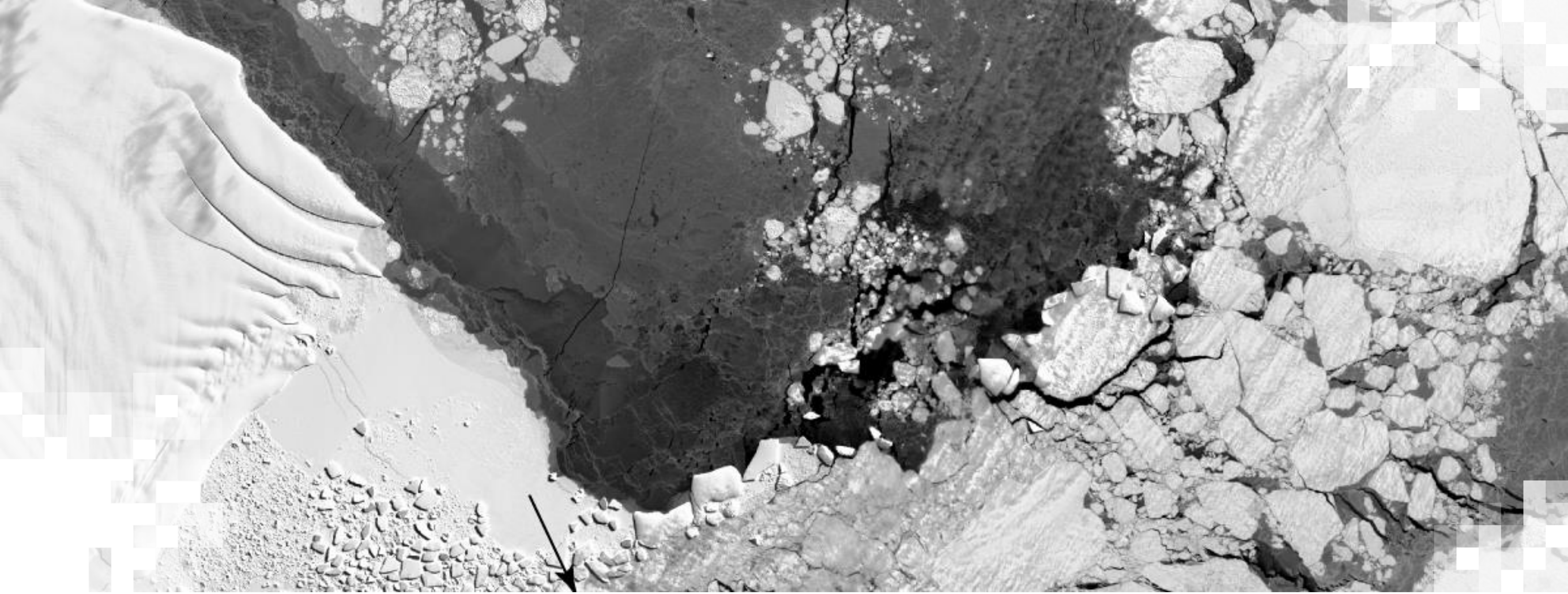

Session 2:

Measuring Surface Subsidence due to Groundwater Extraction with InSAR

Session 2 Objectives

By the end of Part 2, participants will be able to:

- Understand the basic physics of SAR interferometry
- Describe what SAR interferometric phase tells us about the land surface and subsidence
- Describe the data processing required to analyze a time series of SAR interferometry measurements
- Understand the information SAR interferometric images and time series reveal about land subsidence due to groundwater extraction

Prerequisites from ARSET

- Basics of Synthetic Aperture Radar 2017
- SAR Processing and Data Analysis 2017
- Introduction to SAR Interferometry 2017
- Interferometric SAR for Landslide Observations 2019

- Also helpful as it uses the same analysis method:
  – Interferometric SAR Time Series for Landslide Observations 2022

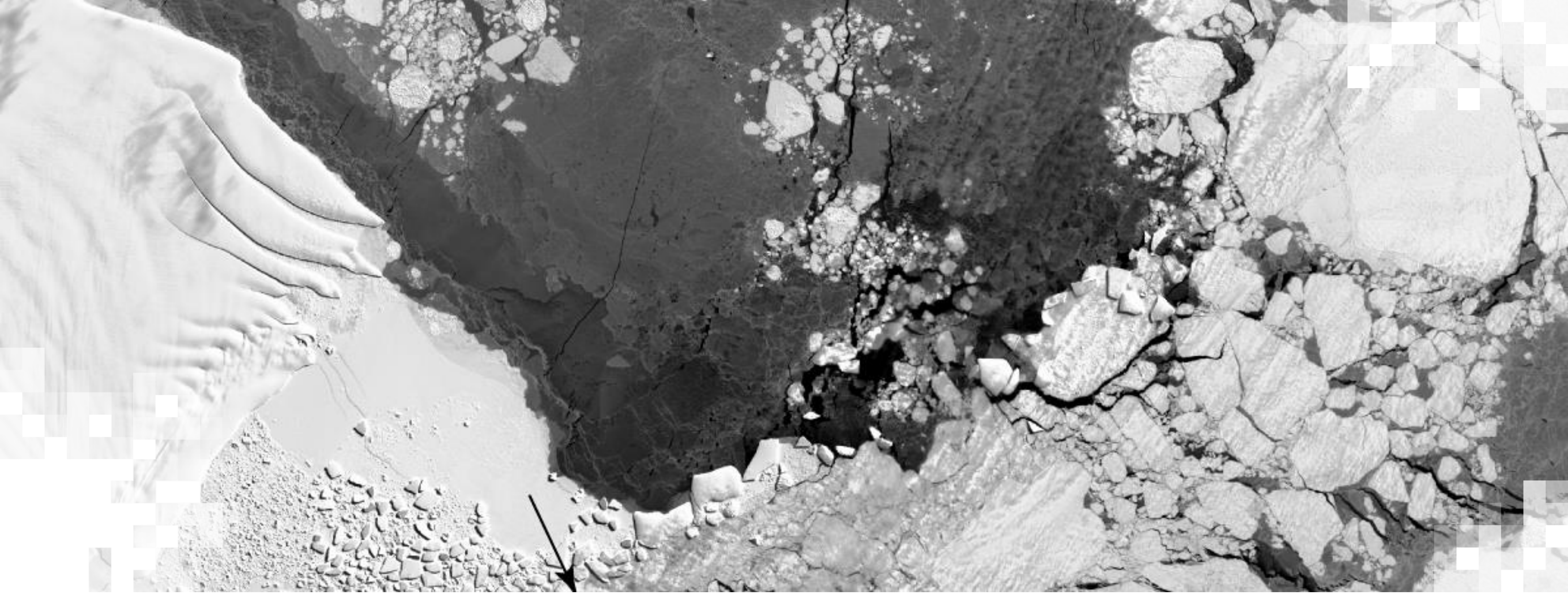

SAR Interferometry Theory (Review)

SAR Interferometry Theory

- Quick review of synthetic aperture radar interferometry theory
- See the 2017 ARSET training "Introduction to SAR Interferometry" and 2019 ARSET training "Interferometric SAR for Landslide Observations" for more details
- In SAR interferometry, it is all about the phase of the SAR signal

SAR Phase – A Measure of Range and Surface Complexity

The phase of the radar signal is the number of **cycles of oscillation** that the wave executes between the radar and the surface and back again.

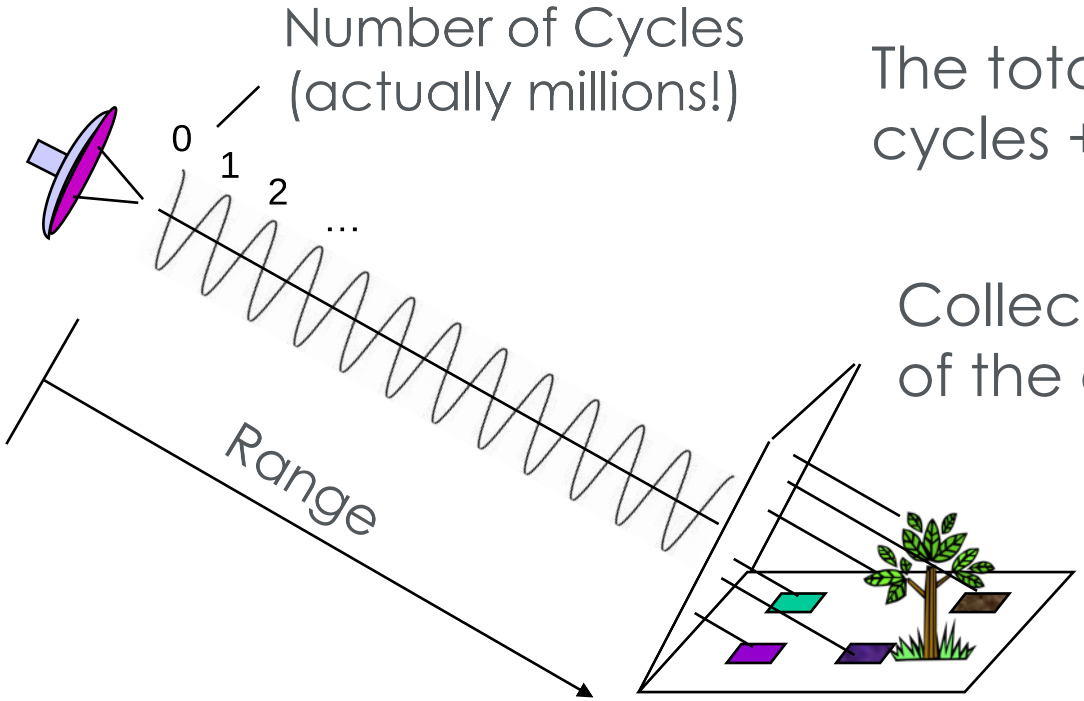

The total phase is a two-way range measured in wave cycles + random components from the surface.

Collection of random path lengths jumbles the phase of the echo.

Only **interferometry** can sort it out!

Slide modified from Paul Rosen (JPL)

A Simplistic View of SAR Phases

Phase of Image 1 $$\phi_1 = \frac{4\pi}{\lambda} \cdot \rho_1 + other\ constants + n_1$$

Phase of Image 2 $$\phi_2 = \frac{4\pi}{\lambda} \cdot \rho_2 + other\ constants + n_2$$

1. The “other constants” cannot be directly determined.
2. “Other constants” depends on scatterer distribution in the resolution cell, which is unknown and varies from cell to cell.
3. The only way of observing the range change is through interferometry (cancellation of “other constants”).

Slide modified from Paul Rosen (JPL)

SAR Interferometry Applications – Mapping

- **Mapping/Cartography**
  - SAR interferometry was used for the 2000 Shuttle Radar Topography Mission (SRTM), new 2018 release as NASADEM.
  - Radar Interferometry from airborne platforms is routinely used to produce topographic maps as digital elevation models (DEMs).
    - 2–5 m circular position accuracy
    - 5–10 m post spacing and resolution
    - 10 km by 80 km DEMs produced in 1 hr on a mini-supercomputer
    - NASA SAR topography presently acquired by GLISTIN
  - Radar imagery is automatically geocoded, becoming easily combined with other (multispectral) data sets.
  - Applications of topography enabled by interferometric rapid mapping:
    - Land use management, classification, hazard assessment, intelligence, urban planning, short and long time scale geology, hydrology

Slide modified from Paul Rosen (JPL)

SAR Interferometry Applications – Changes

- **Deformation Mapping and Change Detection**
  - Repeat-pass radar interferometry from spaceborne platforms is routinely used to produce surface change maps as digital displacement models (DDMs).
    - 0.1–1 centimeter relative displacement accuracy
    - 10–100 m post spacing and resolution
    - 10–350 km wide DDMs produced rapidly once data is available
  - Applications include:
    - Earthquake and volcano monitoring and modeling
    - Landslides and ground subsidence
    - Glacier and ice sheet dynamics
    - Deforestation, change detection, disaster monitoring

Differential Interferometry

- When two observations are made from the same location in space but at different times, the interferometric phase is proportional to any change in the range or distance of a surface feature directly.

$$\Delta\phi = \frac{4\pi}{\lambda}\left(r(t_1) - r(t_2)\right) = \frac{4\pi}{\lambda}\Delta r_{\text{change}}$$

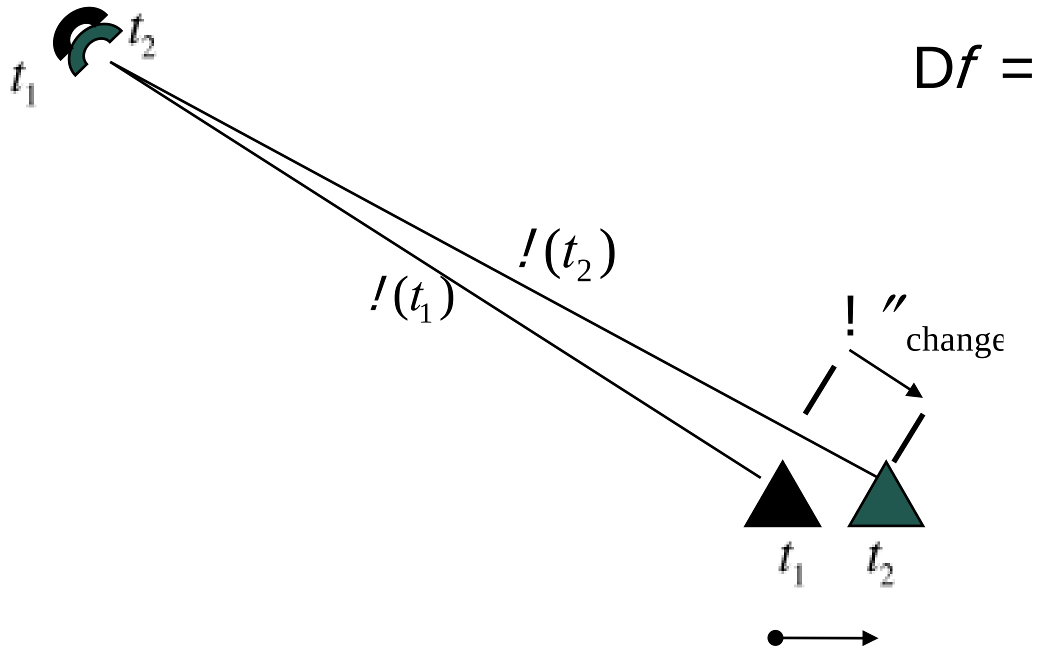

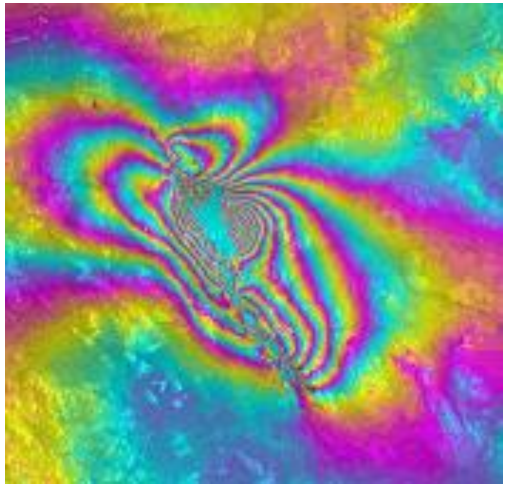

Slide modified from Paul Rosen (JPL)

Differential Interferometry Sensitivities

- The reason differential interferometry can detect millimeter-level surface deformation is that the differential phase is much more sensitive to displacements than to topography.

$$\frac{\partial\phi}{\partial h} = \frac{2\pi p b\cos(\theta-\alpha)}{\lambda\rho\sin\theta} = \frac{2\pi p b_\perp}{\lambda\rho\sin\theta}$$ Topographic Sensitivity

(f ⇔ Df) $$\frac{\partial\phi}{\partial\Delta\rho} = \frac{4\pi}{\lambda}$$ Displacement Sensitivity

$$\sigma_{\phi_{topo}} = \frac{\partial\phi}{\partial h}\sigma_h = \frac{4\pi}{\lambda}\frac{b_\perp}{\rho\sin\theta}\sigma_h$$ Topographic Sensitivity Term

$$\sigma_{\phi_{disp}} = \frac{\partial\phi}{\partial\Delta\rho}\sigma_{\Delta\rho} = \frac{4\pi}{\lambda}\sigma_{\Delta\rho}$$ Displacement Sensitivity Term

Since $\frac{b}{\rho} << 1$ ==> $\frac{\sigma_{\phi_{disp}}}{\sigma_{\Delta\rho}} >> \frac{\sigma_{\phi_{topo}}}{\sigma_h}$

Meter Scale Topography Measurement - Millimeter Scale Topographic Change

Slide modified from Paul Rosen (JPL)

Phase Unwrapping

- From the measured, wrapped phase, unwrap the phase from some arbitrary starting location, then determine the proper 2-pi phase “ambiguity”.

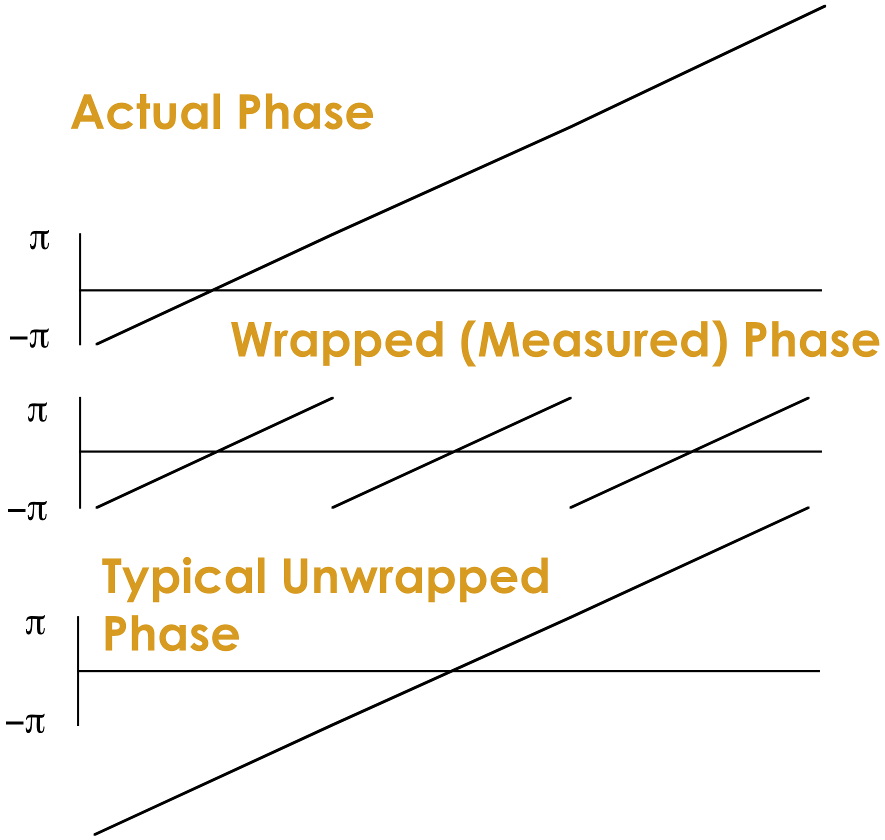

$$\Delta\phi_{topo} = \frac{2\pi p}{\lambda}\left(\rho_1 - \rho_2\right) = \frac{2\pi p}{\lambda}\vec{b} \bullet \vec{l}$$

$$\Delta\phi_{meas} = \mathrm{mod}\left(\Delta\phi_{topo}, 2\pi\right)$$

$$\Delta\phi_{unwrap}(s,\rho) = \Delta\phi_{topo}(s,\rho) + \Delta\phi_{const}$$

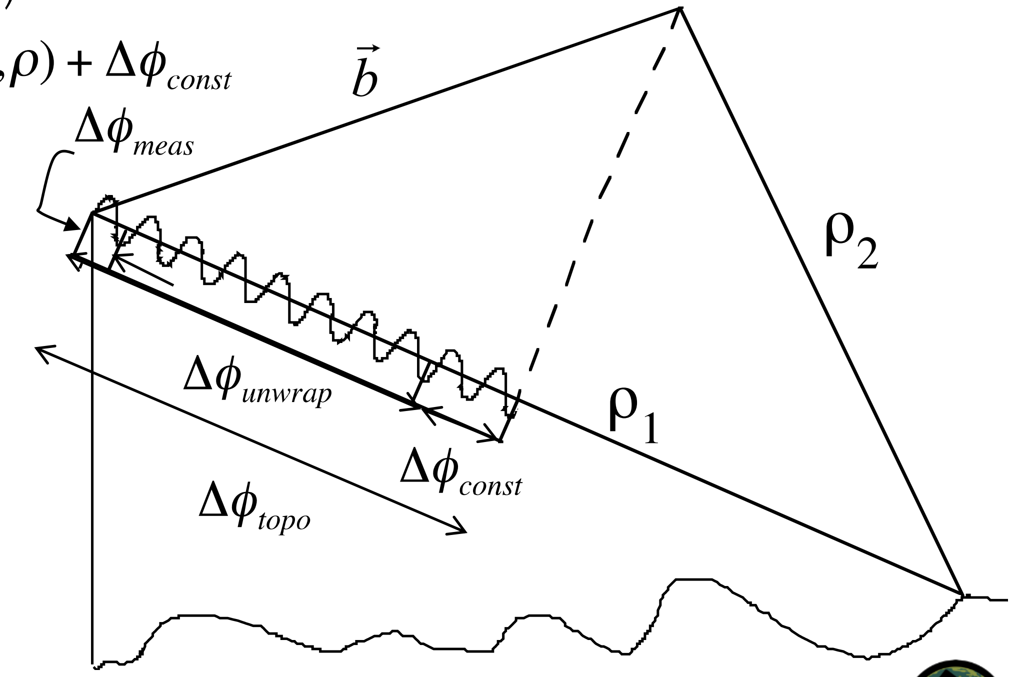

Correlation* Theory

- InSAR signals decorrelate (become incoherent) due to:
  - Thermal and Processor Noise
  - Differential Geometric and Volumetric Scattering
  - Rotation of Viewing Geometry
  - Random Motions Over Time

- Decorrelation relates to the local phase standard deviation of the interferogram phase.
  - Affects height and displacement accuracy
  - Affects ability to unwrap phase

*"Correlation" and "Coherence" are often used synonymously.

Slide modified from Paul Rosen (JPL)

InSAR Correlation Components

- Correlation effects multiply, unlike phase effects that add.
- Low coherence or decorrelation for any reason causes loss of information in that area.

$$\gamma = \gamma_v \gamma_g \gamma_t \gamma_c$$

Where:
γ_v is volumetric (trees)
γ_g is geometric (steep slopes)
γ_t is temporal (gradual changes)
γ_c is sudden changes

Wavelength: A Measure of Surface Scale

Light interacts most strongly with objects around the size of the wavelength.

L (24 cm) C (6 cm) X (3 cm)

Forest: Leaves reflect X-band wavelengths but not L-band.

Dry Soils: Surface looks rough to X-band but not L-band.

Ice: Surface and layering look rough to X-band but not L-band.

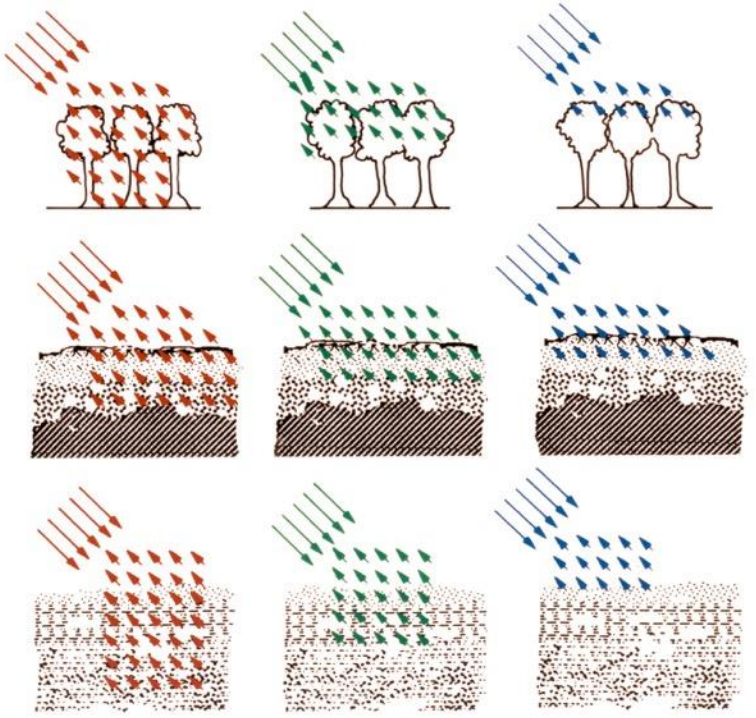

Slide modified from Paul Rosen (JPL)

InSAR Coherence and Wavelength

- SIR-C L- and C-band Interferometry
- 6-month time separated observations to form interferograms
- Simultaneous C and L band

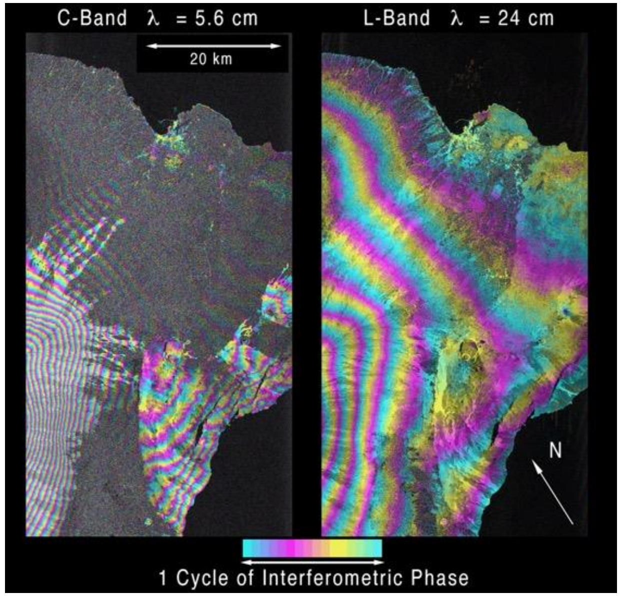

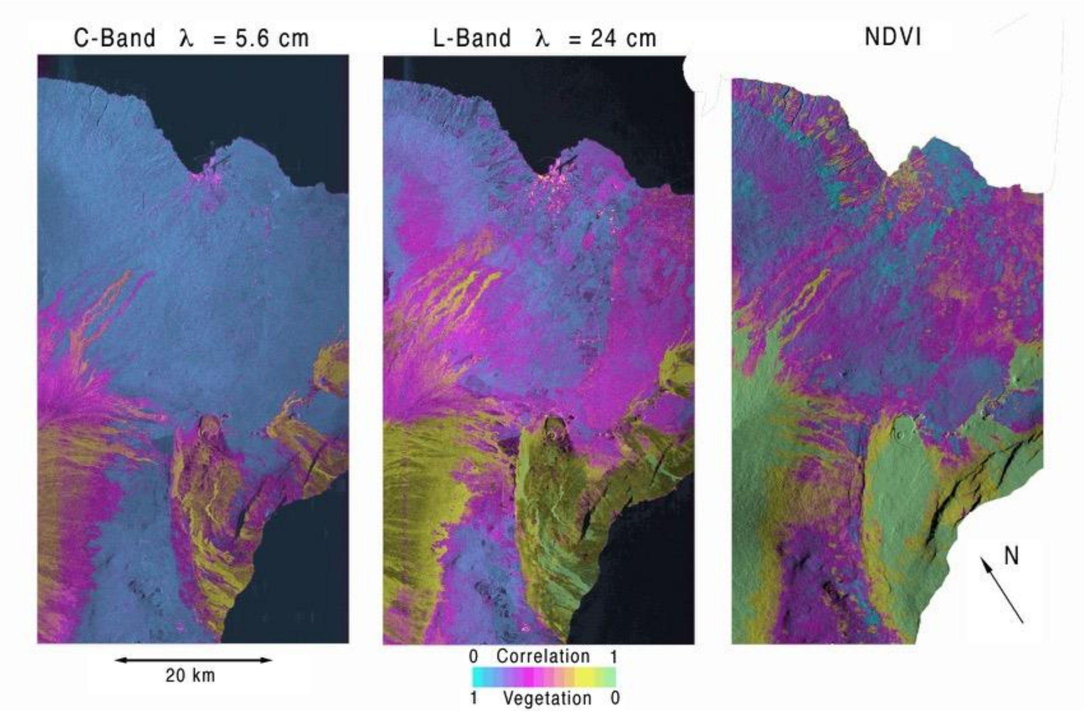

InSAR experiments have shown good correlation at L-band.

Rosen, P. A., S. Hensley, H. A. Zebker, F. H. Webb, and E. J. Fielding (1996). Surface deformation and coherence measurements of Kilauea Volcano, Hawaii, from SIR-C radar interferometry, Journal of Geophysical Research 101, no. E10, 23109-23125, doi:10.1029/96JE01459.

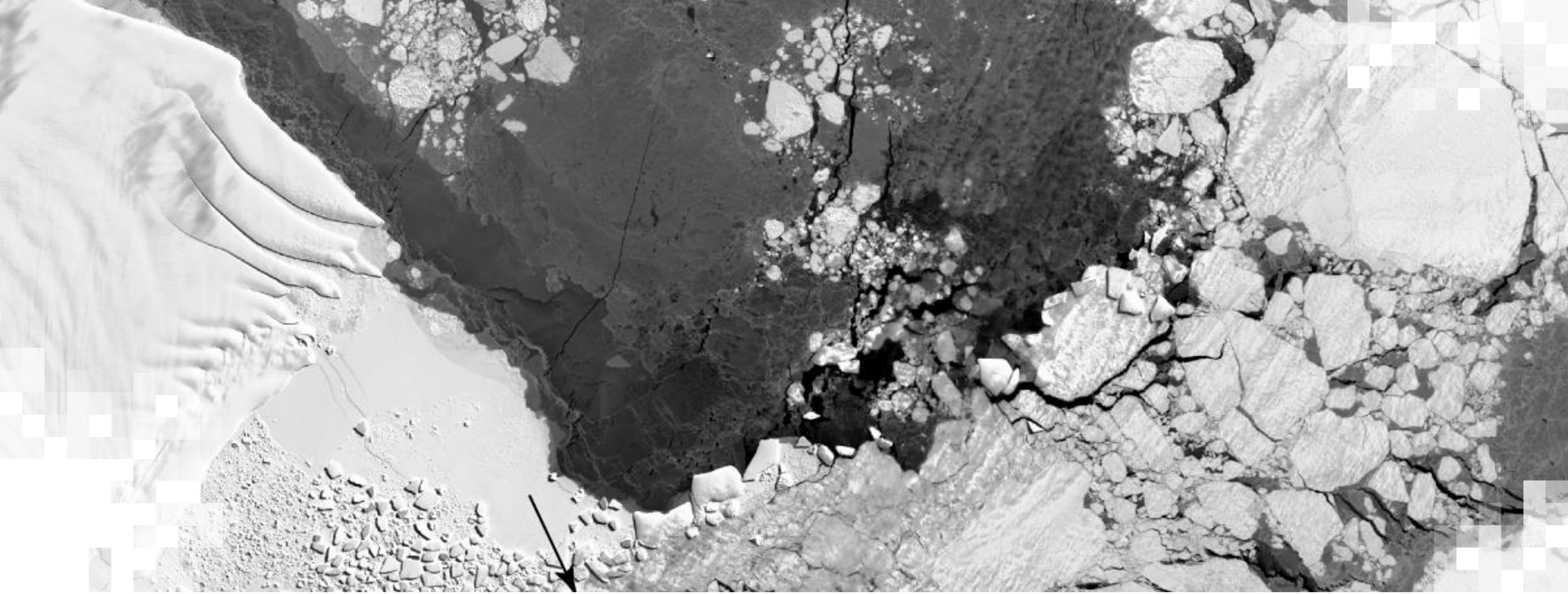

SAR Data for Ground Subsidence

SAR Satellites

Satellite (Launch and End of Operations)	Repeat Cycle (Days)	Wave-length (cm)
European ERS-1/ERS-2 ‘92-’01(-2011)	35 (1,3,183)	6
Canadian RADARSAT-1 1995-2013	24	6
European Envisat ‘03-Sep.’10(‘10-Apr.’12)	35 (30)	6
Japanese ALOS Jan. 2006–Apr. 2011	46	24
German TerraSAR-X ’07–, TanDEM-X ’10–	11	3
Italian COSMO-SkyMed 4x launch ‘07-’10 (one deorbited ‘21)	16 (1,4,7,8)	3
Canadian RADARSAT-2 launched Dec. 2007–	24	6

New SAR Spacecraft – Part 1

Satellite (Launch or Planned)	Repeat Cycle (Days)	Wave-length (cm)
Copernicus Sentinel-1 (A: Apr. 2014, B: Apr. 2016–Dec. 2021, C: 2024?)	12(6)	6
Japanese ALOS-2 (May 2014)	14	24
Indian RISAT-1 (Apr. 2012–2017)	25	6
NASA-ISRO SAR (NISAR) mission (2024)	12	12,24

New SAR Spacecraft – Part 2

Satellite (Launch or Planned)	Repeat Cycle (Days)	Wave-length (cm)
Argentina SAOCOM-1 (A: Oct. 2018, B: Aug. 2020)	16(8)	24
Japanese ALOS-4 (Mar. 2024?)	14	24
Italian COSMO-SkyMed Next Gen. (1: Dec. 2019, 2: Jan. 2022, 3:, 4:)	16	3
Canadian RADARSAT Constellation Mission 3x (Jun. 2019)	4	6

New SAR Spacecraft – Part 3

Satellite (Launch or Planned)	Repeat Cycle (Days)	Wave-length (cm)
South Korea KompSat-5 (2013-2022)	16(8)	3
Spanish PAZ (clone TerraSAR-X) (Feb. 2018)	11 (4,7)	3
Capella-1 through -n (2018-Aug. 2023)	N/A	3
ICEYE ~16 satellites now (Aug. 2023) some satellites have 1-day separation	1	3

NASA-ISRO SAR Mission (NISAR)

- High Spatial Resolution with Frequent Revisit Time
- Planned Launch Date: Feb. 2024
- Dual Frequency L- and S-Band SAR
  - L-Band SAR from NASA and S-Band SAR from ISRO
- 3 Years Science Operations (5+ years Consumables)
- All science data will be made available free and open.
- https://nisar.jpl.nasa.gov

NISAR Characteristic:	Would Enable:
L-band (24 cm wavelength)	Low temporal decorrelation and foliage penetration
S-band (12 cm wavelength)	Sensitivity to light vegetation
SweepSAR technique with Imaging Swath >240 km	Global data collection
Polarimetry (Single/Dual/Quad)	Surface characterization and biomass estimation
12-day exact repeat	Rapid Sampling
3-10 meters mode-dependent SAR resolution	Small-scale observations
3 years since operations (5 years consumables)	Time-series analysis
Pointing control < 273 arcseconds	Deformation interferometry
Orbit control < 500 meters	Deformation interferometry
>30% observation duty cycle	Complete land/ice coverage
Left/Right pointing capability	Polar coverage, North and South
Noise Equivalent Sigma Zero ≤ -23 db	Surface characterization of smooth surfaces

Slide courtesy of Paul Rosen (JPL)

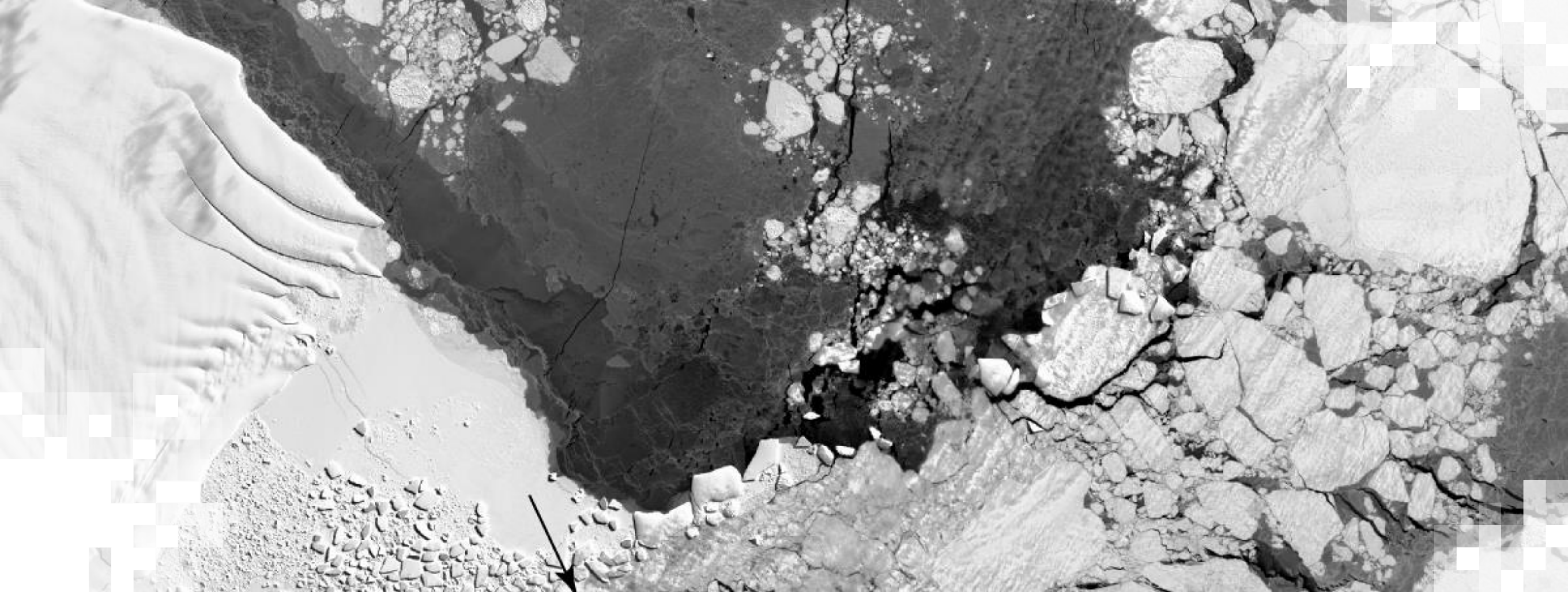

Subsidence Due to Groundwater Extraction

Remote Sensing Land Subsidence from Space

Measurement of crustal deformation is also used to detect land subsidence: sinking of the land due to withdrawal of water and oil.

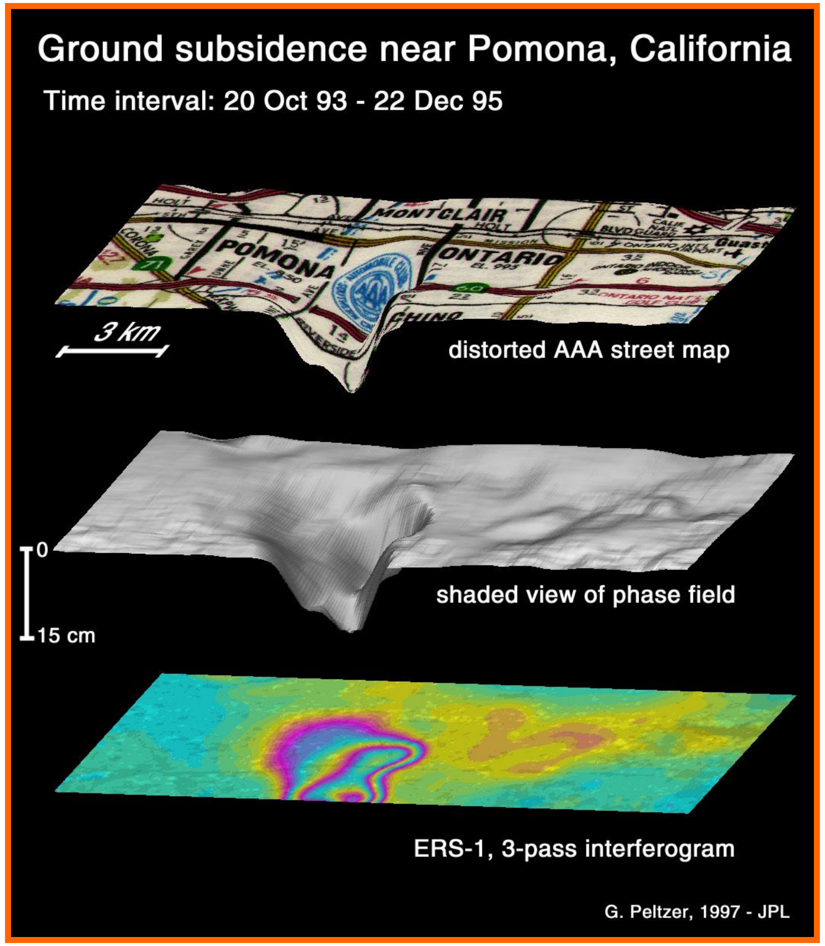

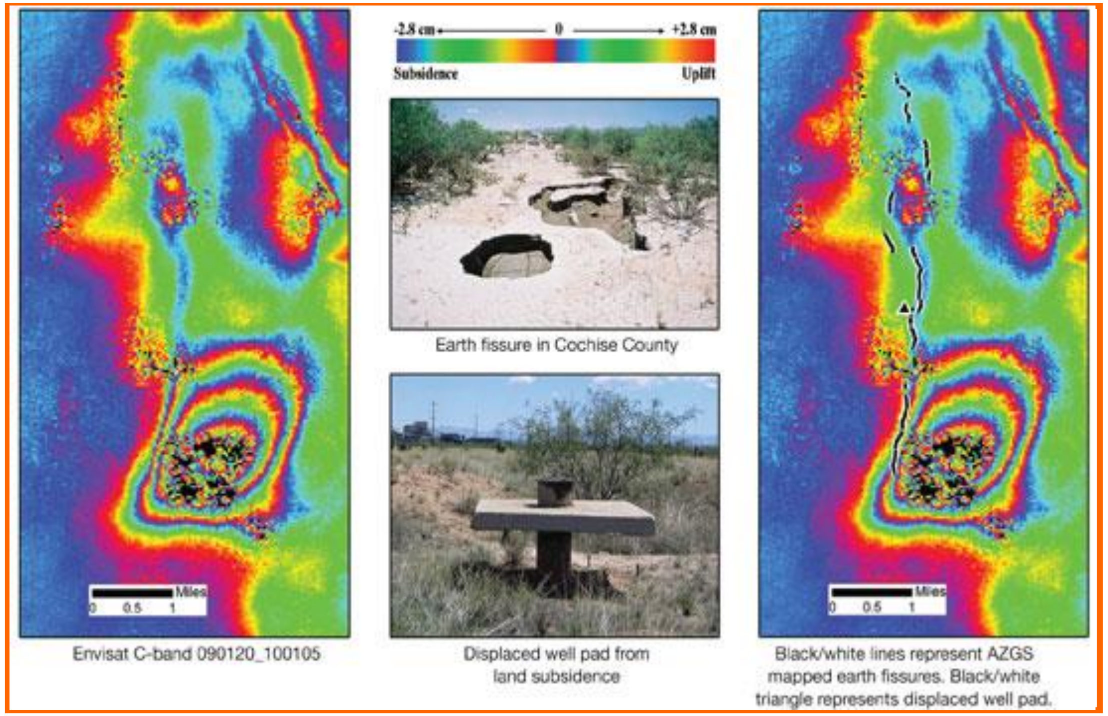

Arizona DWR, the largest annual deformation rate detected (~11cm) using InSAR in Cochise County, SE Arizona. Time interval: Jan 20, 2009-Jan 05, 2010. Conway et al., 2010

Slide by Zhen Liu, Jet Propulsion Laboratory

Aquifer Compaction and Land Subsidence

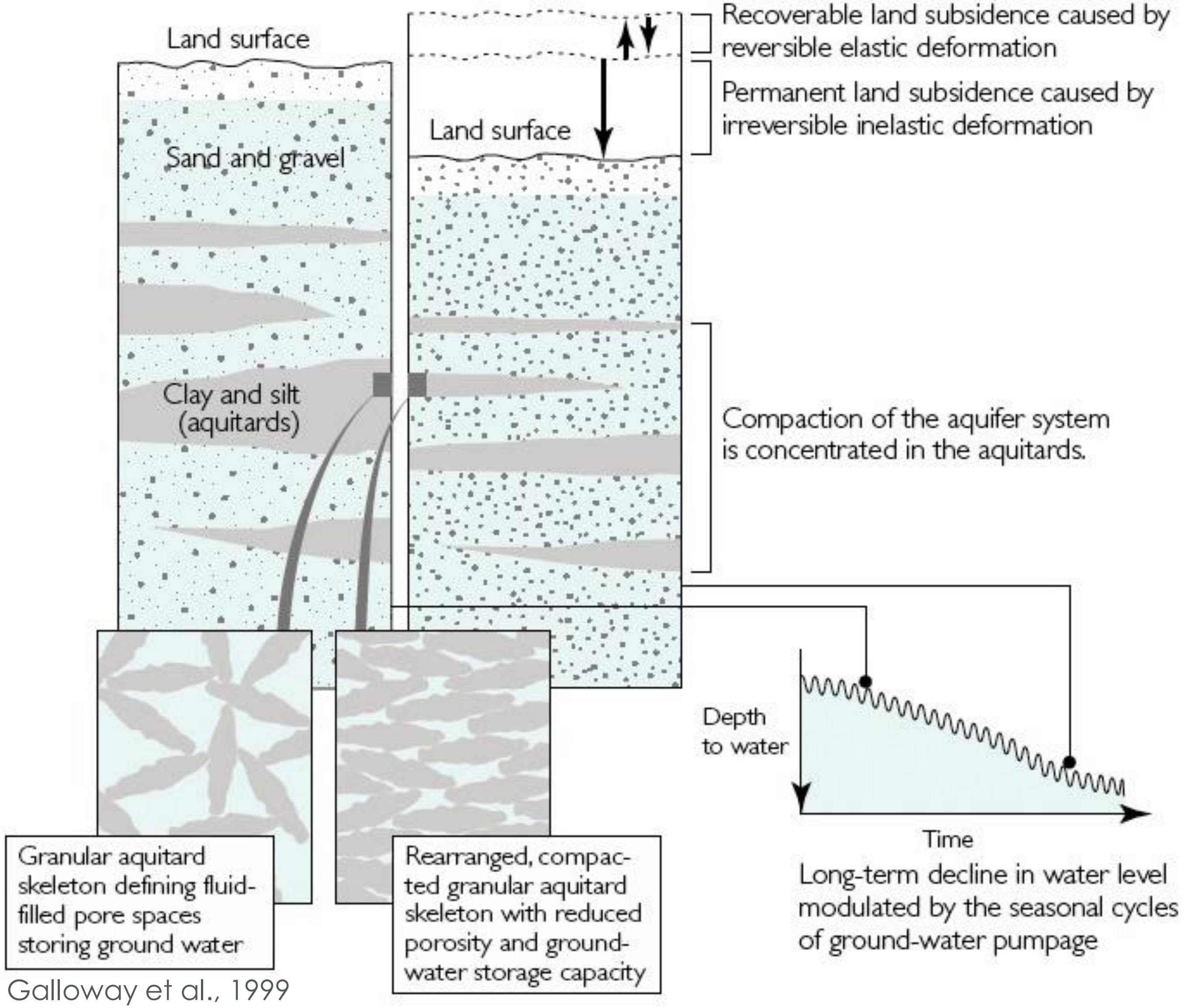

Galloway et al., 1999

Slide by Zhen Liu, Jet Propulsion Laboratory

Seasonal Basin Deformation Due to Groundwater Withdrawal and Recharge

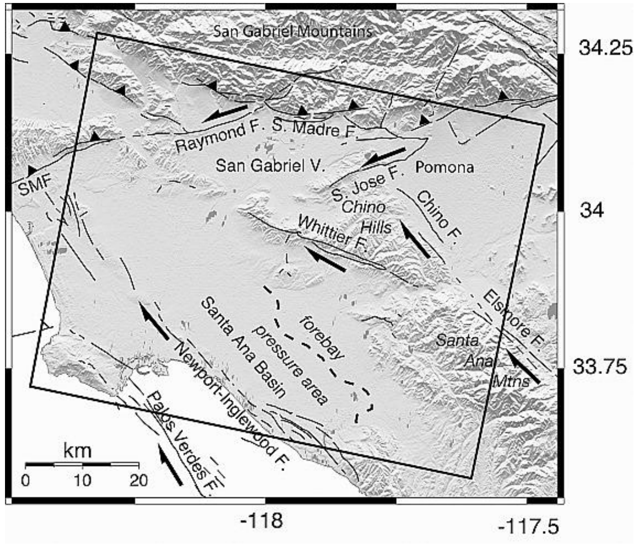

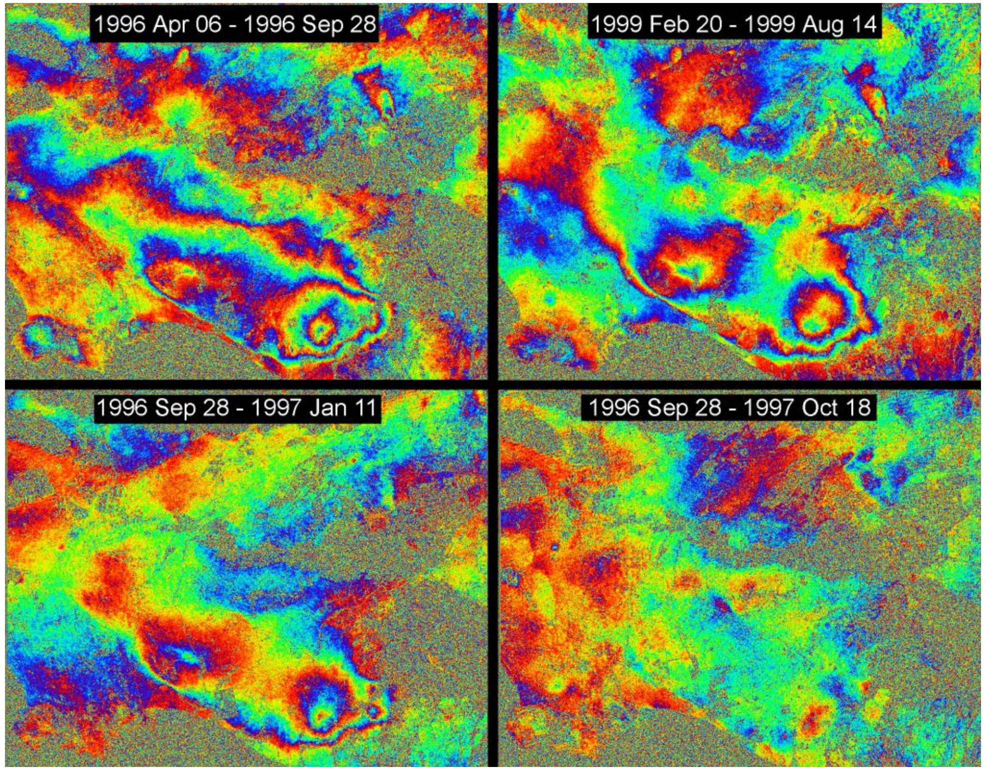

Top Panels: Subsidence in Santa Ana Basin, Summer;
Bottom (Left): Uplift Due to Winter Water Recharge;
(Right) : Neutral Over One-Year Span

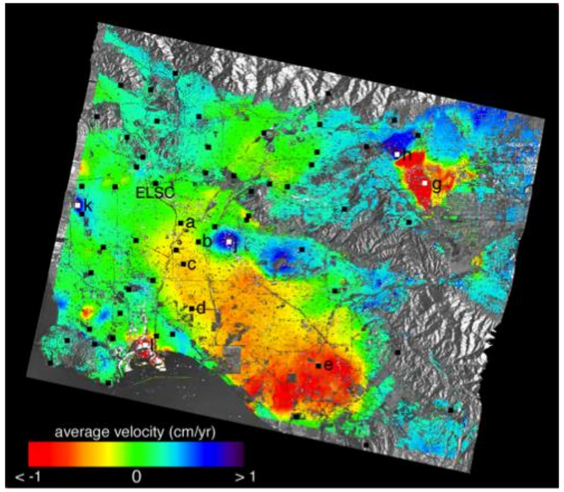

Average Ground Velocities in the Radar Line-Of-Sight (LOS)

Lanari, R. P. Lundgren, M. Manzo, F. Casu (2004), Satellite radar interferometry time series analysis of surface deformation for Los Angeles, California, Geophys. Res. Lett., 31, L23613, doi:10.1029/2004GL021294

Slide by Zhen Liu, Jet Propulsion Laboratory

The Central Valley of California

- **Central Valley Facts:**
  - California's Central Valley covers about 20,000 square miles.
  - Structural Trough: ~400 miles long and 20-70 miles wide, partially filled marine deposits overlaying with continental sediments
  - One of the most productive agriculture regions in the world with > 250 different crops grown in the Central Valley, and an estimated annual output value of ~$17 billion
  - Approximately one-sixth of US irrigated land is in the Central Valley.
  - About one-fifth of US groundwater pumpage is from the Central Valley aquifer system.

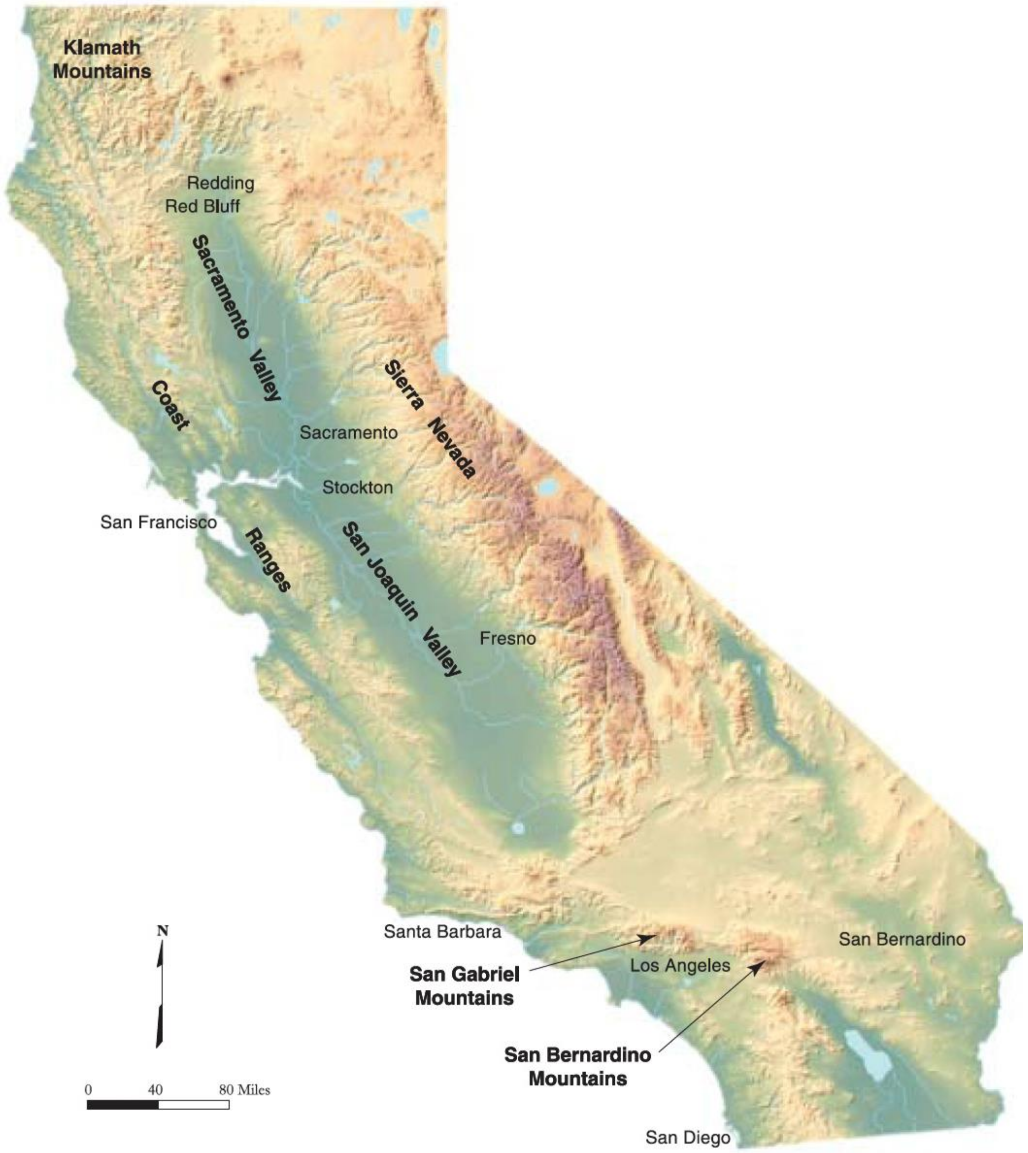

Slide by Zhen Liu, Jet Propulsion Laboratory

ALOS PALSAR Time Series Compared with Well Data

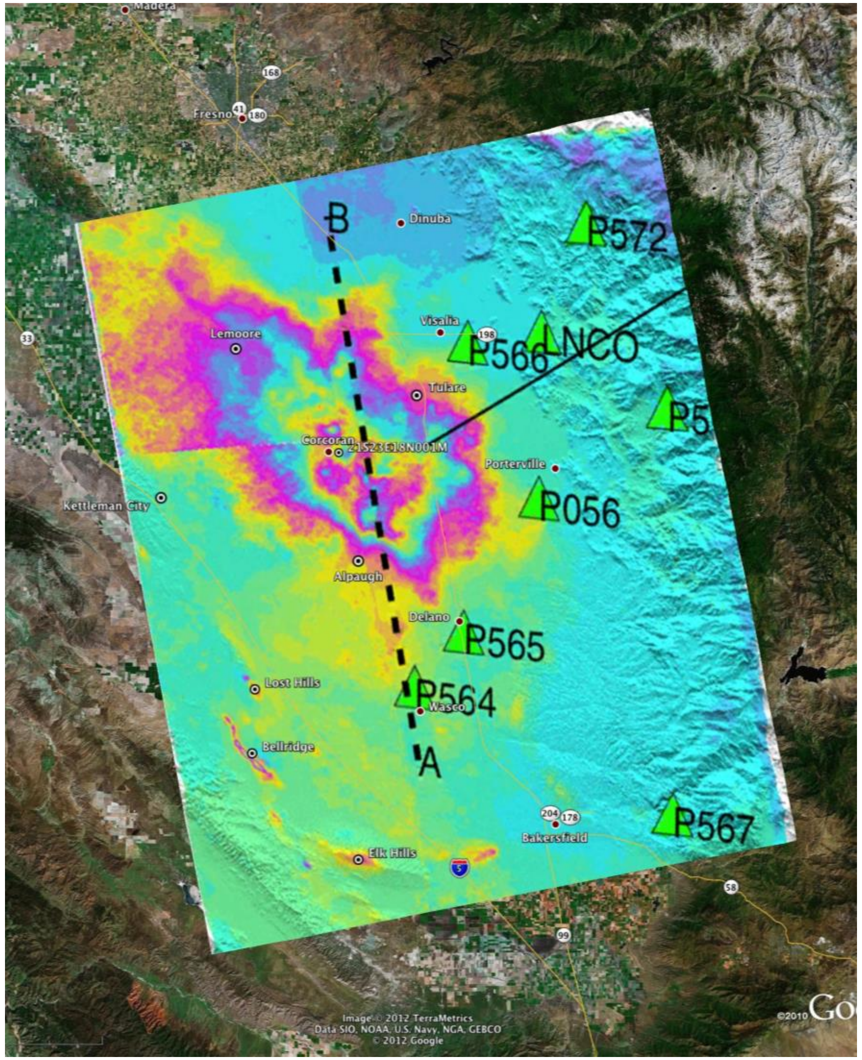

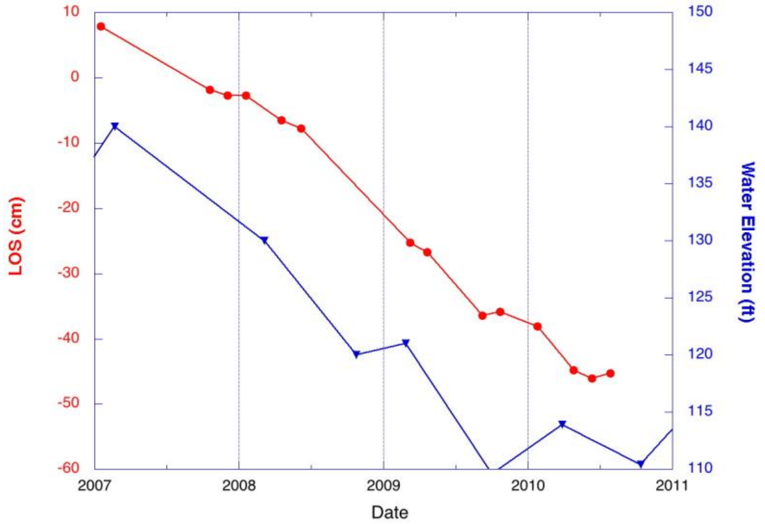

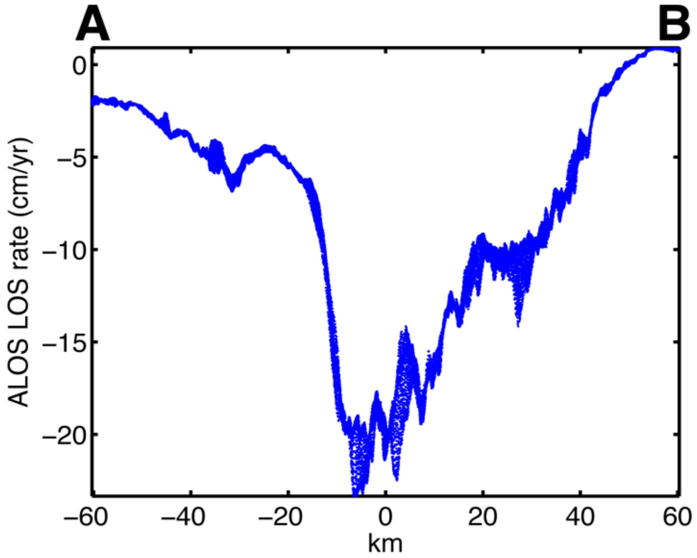

PALSAR 2007–2011 matches generally with well data, but both time series are sparse.

Slide by Zhen Liu, Jet Propulsion Laboratory

Subsidence in the Central Valley of California: PALSAR, 2007-2011

Zhen Liu, Vince Realmuto, Tom Farr, JPL

Comparison of InSAR, GPS, and Water Surface Elevation in Wells

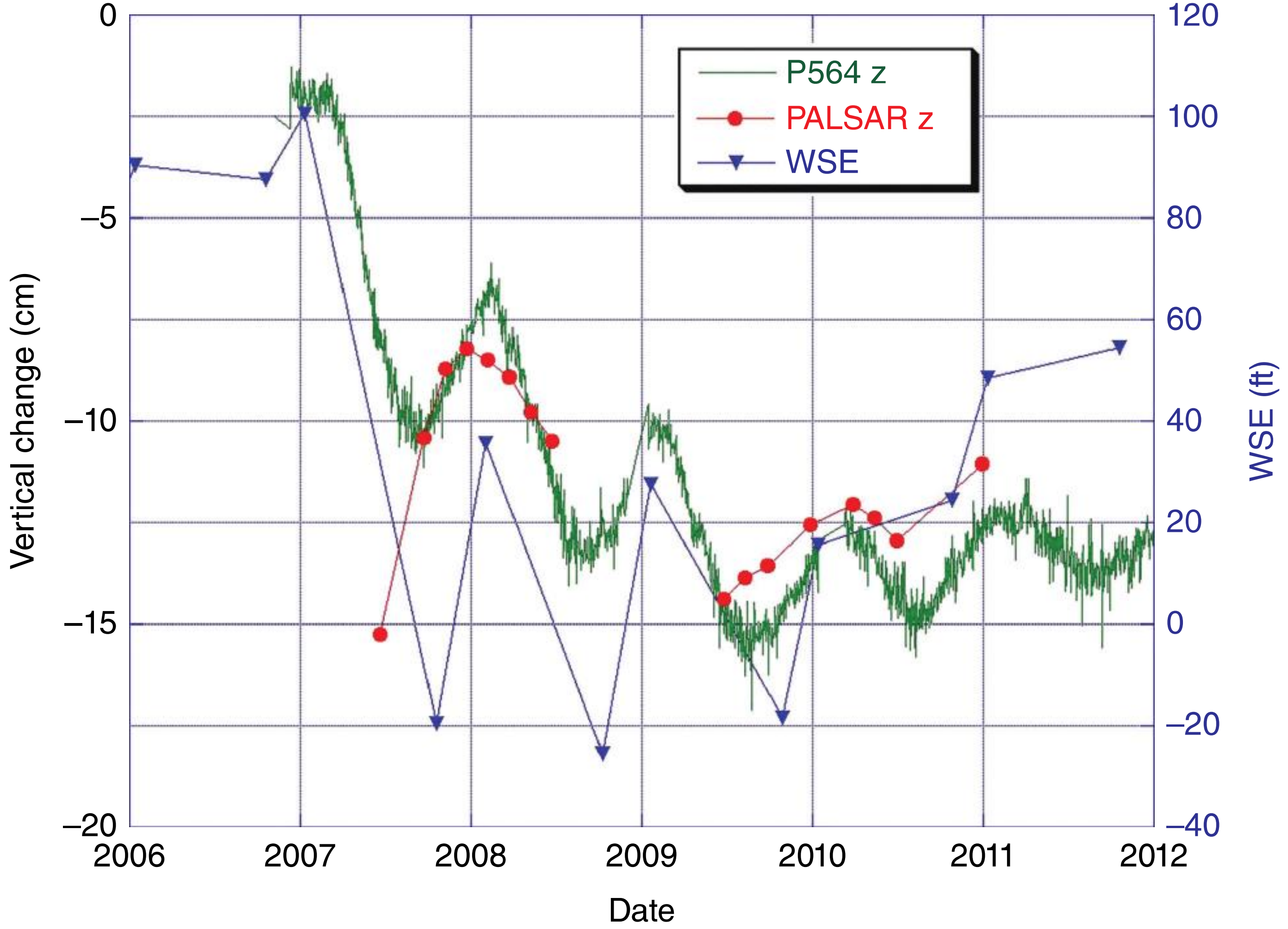

Farr, T., Z. Liu, 2015, Monitoring Groundwater in the Central Valley of California with Interferometric Radar, *AGU Chapman Monograph for remote sensing*, 397-406, DOI:10.1002/9781118872086.ch24.

Slide by Zhen Liu, Jet Propulsion Laboratory

California Drought Response – 2015

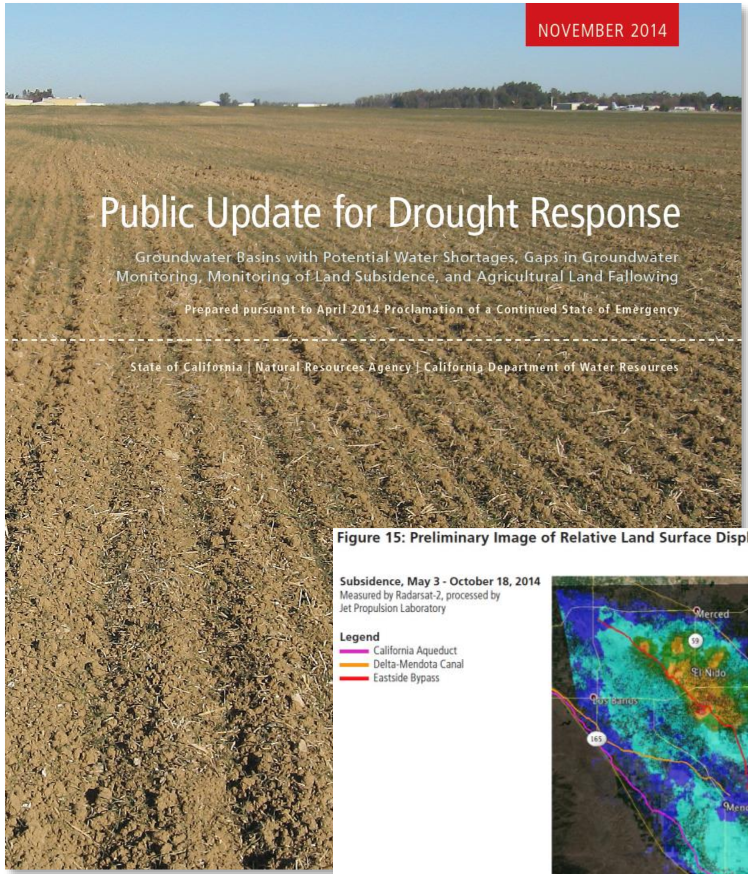

Figure 15: Preliminary Image of Relative Land Surface Displacement, San Joaquin Valley - May to October 2014.

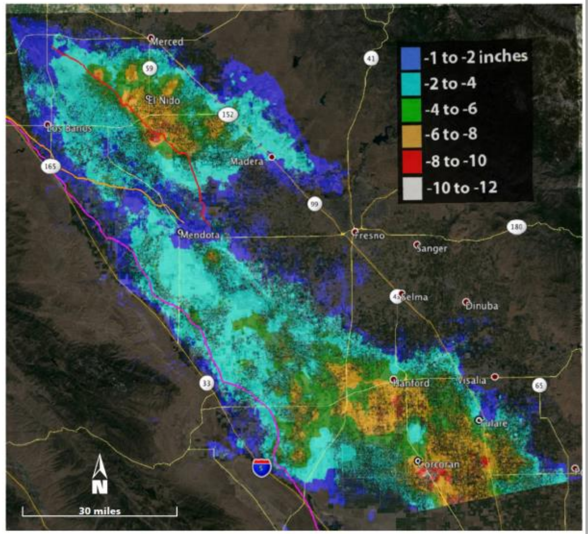

http://water.ca.gov/waterconditions/index.cfm

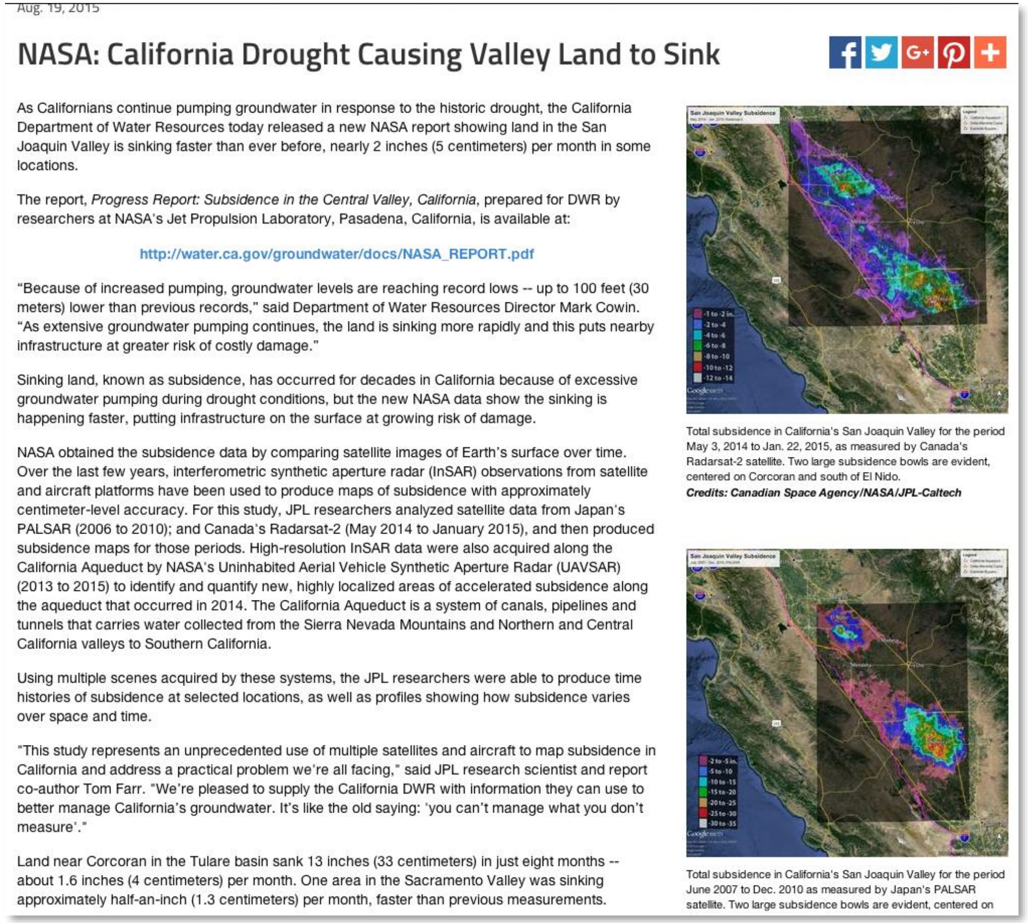

Aug. 19, 2015

NASA: California Drought Causing Valley Land to Sink

As Californians continue pumping groundwater in response to the historic drought, the California Department of Water Resources today released a new NASA report showing land in the San Joaquin Valley is sinking faster than ever before, nearly 2 inches (5 centimeters) per month in some locations.

The report, *Progress Report: Subsidence in the Central Valley, California*, prepared for DWR by researchers at NASA's Jet Propulsion Laboratory, Pasadena, California, is available at:

http://water.ca.gov/groundwater/docs/NASA_REPORT.pdf

"Because of increased pumping, groundwater levels are reaching record lows -- up to 100 feet (30 meters) lower than previous records," said Department of Water Resources Director Mark Cowin. "As extensive groundwater pumping continues, the land is sinking more rapidly and this puts nearby infrastructure at greater risk of costly damage."

Sinking land, known as subsidence, has occurred for decades in California because of excessive groundwater pumping during drought conditions, but the new NASA data show the sinking is happening faster, putting infrastructure on the surface at growing risk of damage.

NASA obtained the subsidence data by comparing satellite images of Earth's surface over time. Over the last few years, interferometric synthetic aperture radar (InSAR) observations from satellite and aircraft platforms have been used to produce maps of subsidence with approximately centimeter-level accuracy. For this study, JPL researchers analyzed satellite data from Japan's PALSAR (2006 to 2010); and Canada's Radarsat-2 (May 2014 to January 2015), and then produced subsidence maps for those periods. High-resolution InSAR data were also acquired along the California Aqueduct by NASA's Uninhabited Aerial Vehicle Synthetic Aperture Radar (UAVSAR) (2013 to 2015) to identify and quantify new, highly localized areas of accelerated subsidence along the aqueduct that occurred in 2014. The California Aqueduct is a system of canals, pipelines and tunnels that carries water collected from the Sierra Nevada Mountains and Northern and Central California valleys to Southern California.

Using multiple scenes acquired by these systems, the JPL researchers were able to produce time histories of subsidence at selected locations, as well as profiles showing how subsidence varies over space and time.

"This study represents an unprecedented use of multiple satellites and aircraft to map subsidence in California and address a practical problem we're all facing," said JPL research scientist and report co-author Tom Farr. "We're pleased to supply the California DWR with information they can use to better manage California's groundwater. It's like the old saying: 'you can't manage what you don't measure'."

Land near Corcoran in the Tulare basin sank 13 inches (33 centimeters) in just eight months -- about 1.6 inches (4 centimeters) per month. One area in the Sacramento Valley was sinking approximately half-an-inch (1.3 centimeters) per month, faster than previous measurements.

Total subsidence in California's San Joaquin Valley for the period May 3, 2014 to Jan. 22, 2015, as measured by Canada's Radarsat-2 satellite. Two large subsidence bowls are evident, centered on Corcoran and south of El Nido.
Credits: Canadian Space Agency/NASA/JPL-Caltech

Total subsidence in California's San Joaquin Valley for the period June 2007 to Dec. 2010 as measured by Japan's PALSAR satellite. Two large subsidence bowls are evident, centered on

http://www.nasa.gov/jpl/nasa-california-drought-causing-valley-land-to-sink

Slide by Zhen Liu, Jet Propulsion Laboratory

Sentinel-1 Measured Subsidence in Central Valley from 2015 to 2017

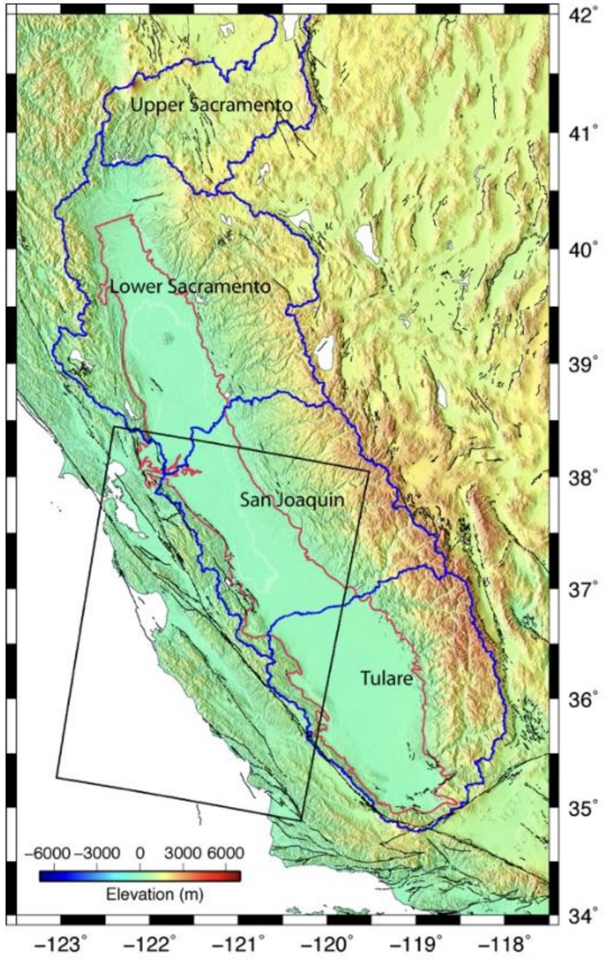

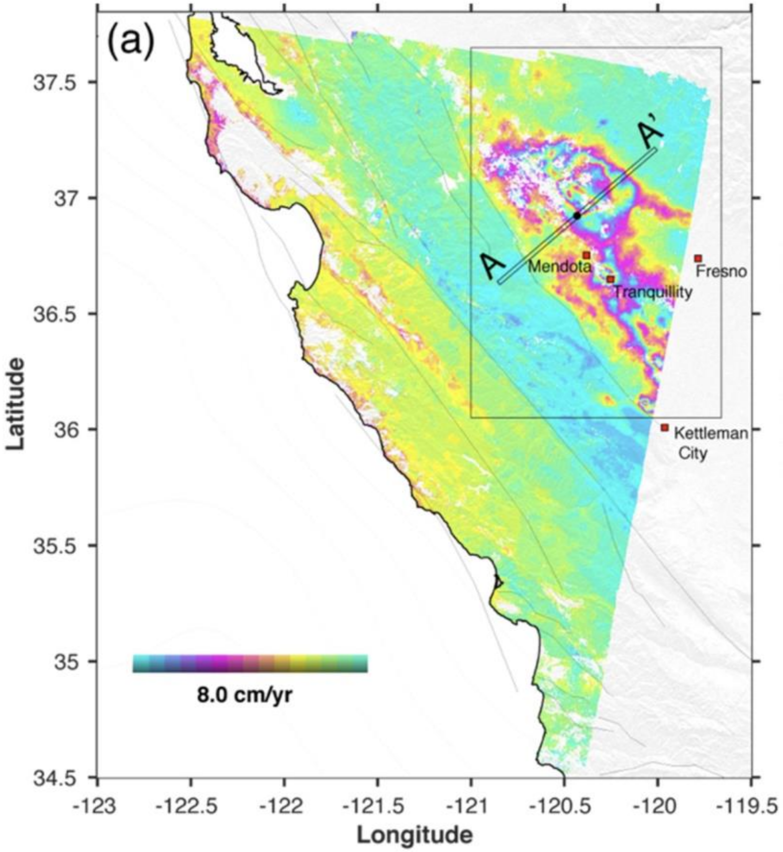

Comparison Between 2015-2017 (S1) and 2006-2010 (ALOS-1)

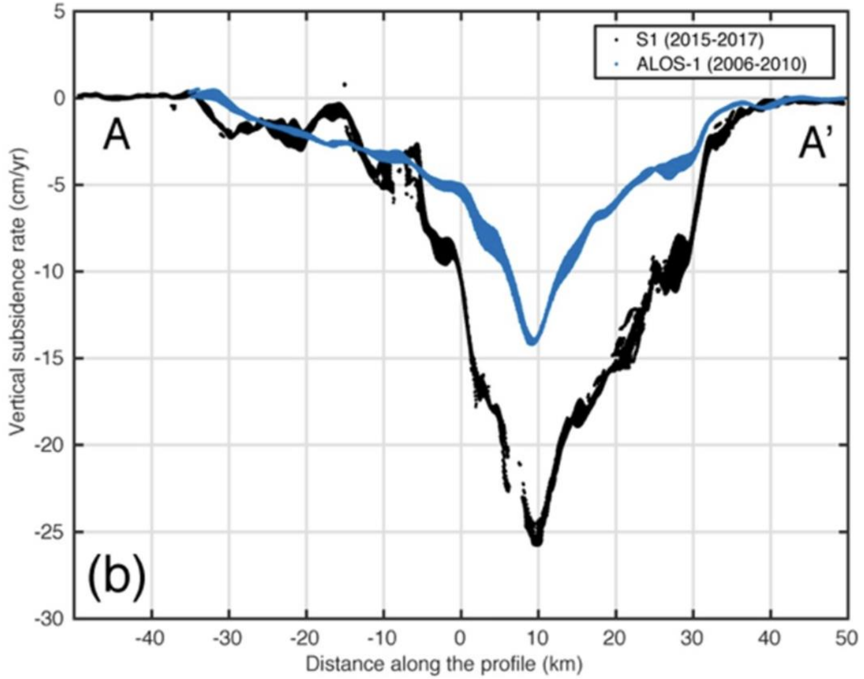

Liu, Z., P.W. Liu, E. Massoud, T. G. Farr, P. Lundgren, J. S. Famiglietti, 2019, Monitoring Groundwater Change in California's Central Valley Using Sentinel-1 and GRACE Observations, *Geosciences*, 9, 436; doi:10.3390/geosciences9100436.

Slide by Zhen Liu, Jet Propulsion Laboratory

Comparison Between InSAR and GPS LOS Time Series

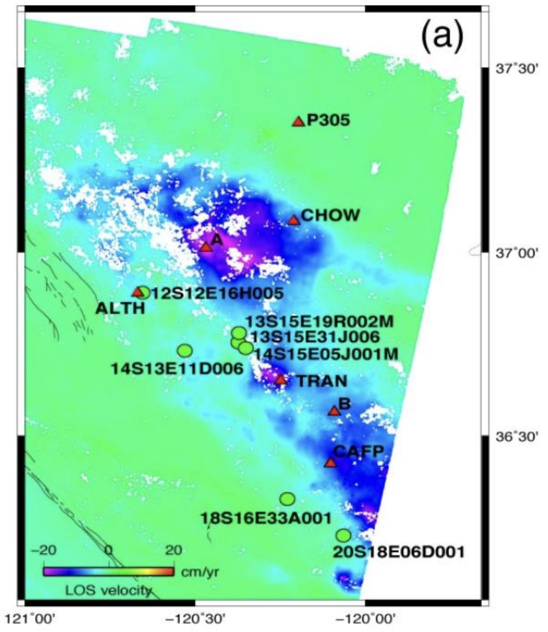

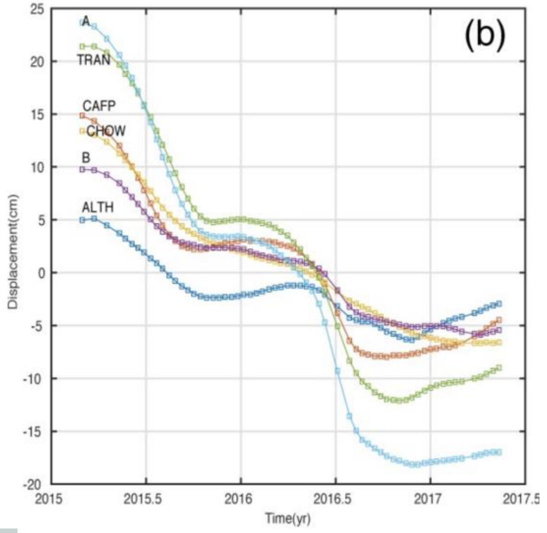

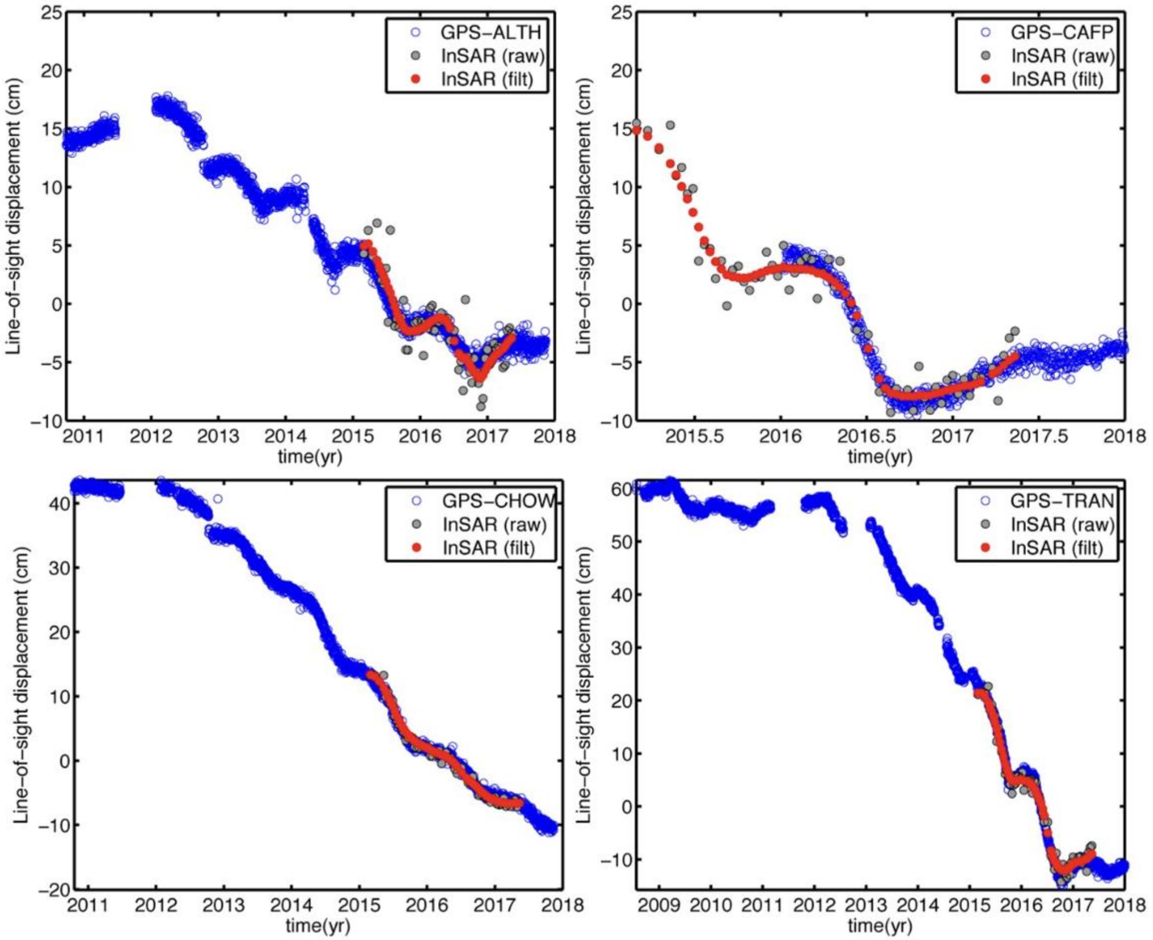

- Similar subsidence history in heavily subsiding area
- Response of Aquifer to drought and seasonal precipitation

Slide by Zhen Liu, Jet Propulsion Laboratory

Comparison of Vertical Subsidence Time Series and Water Surface Elevation in Collocated Well

- Water Surface Elevation (WSE) shows water level in well
- Latency between groundwater recovery (orange) and the cessation of inelastic subsidence (blue) reflects delayed equilibration of aquitard head levels

Liu et al., Geosciences, 2019

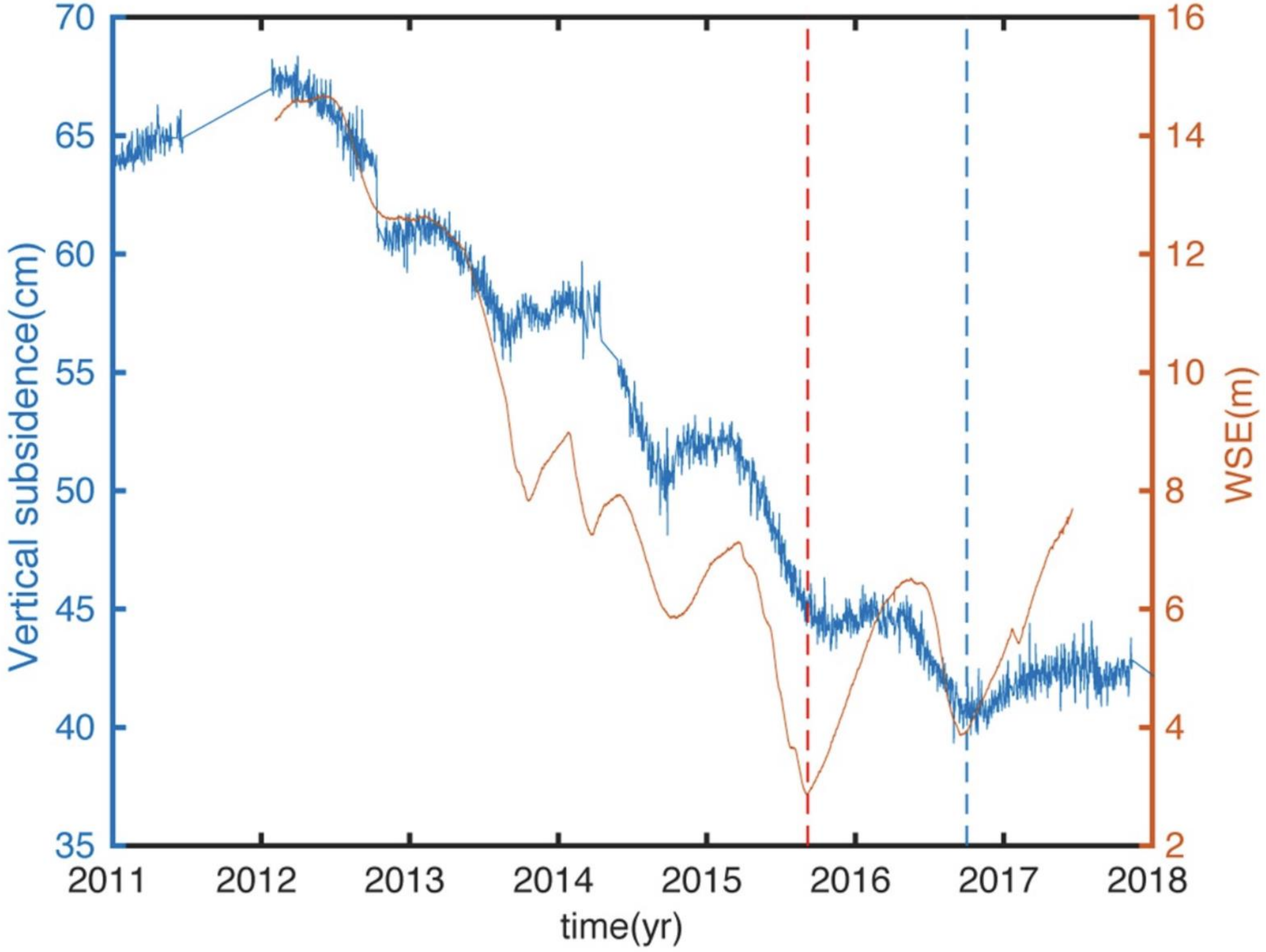

Slide by Zhen Liu, Jet Propulsion Laboratory

Comparison of GRACE, Representative Subsidence, and PRISM Precipitation

- Good agreement between basin-wide GRACE-derived GroundWater Anomaly (GWA) and subsidence over longer time scale
- Irreversible long-term subsidence due to compaction of fine-grained layers

Liu et al., Geosciences, 2019

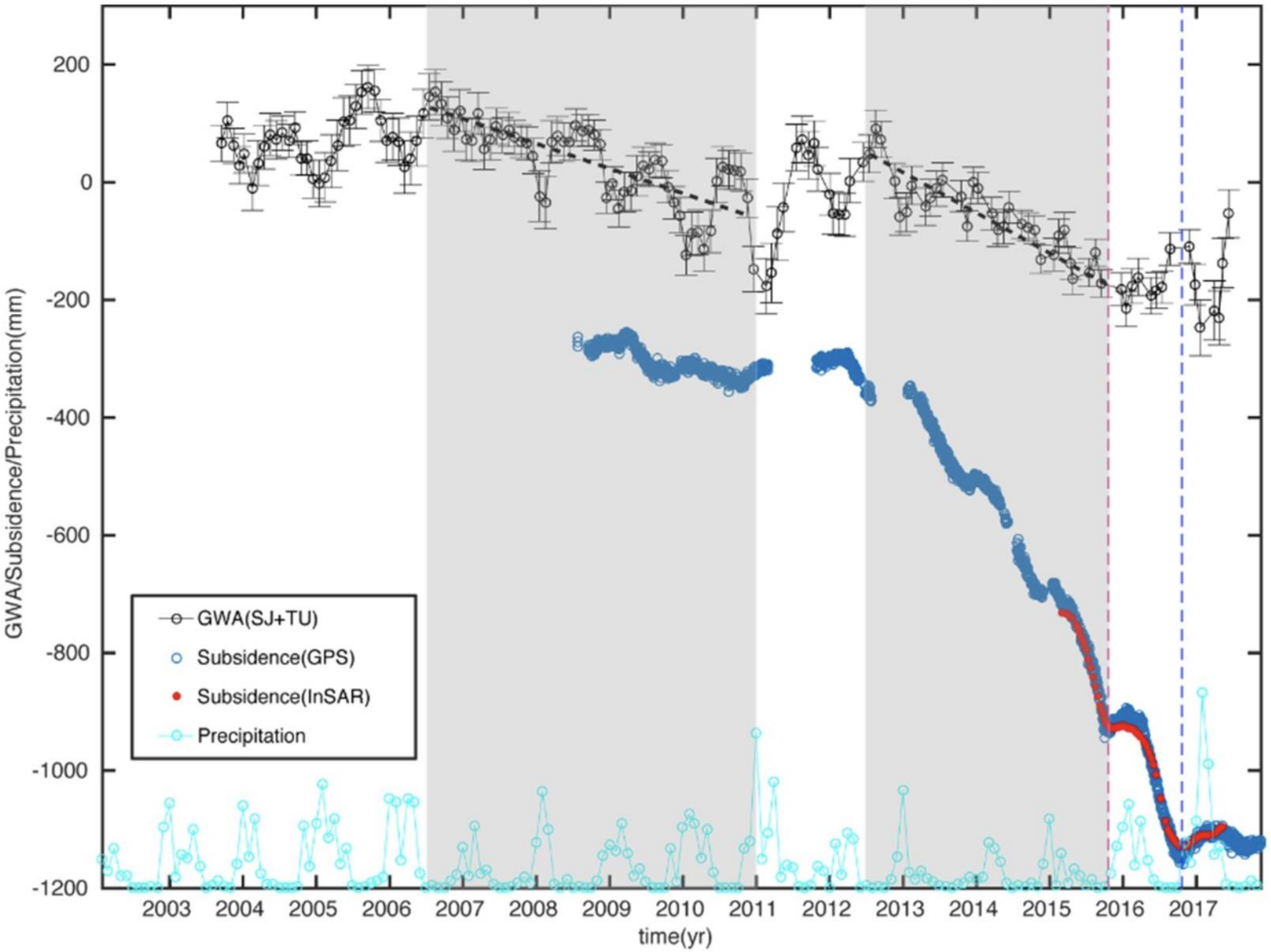

Slide by Zhen Liu, Jet Propulsion Laboratory

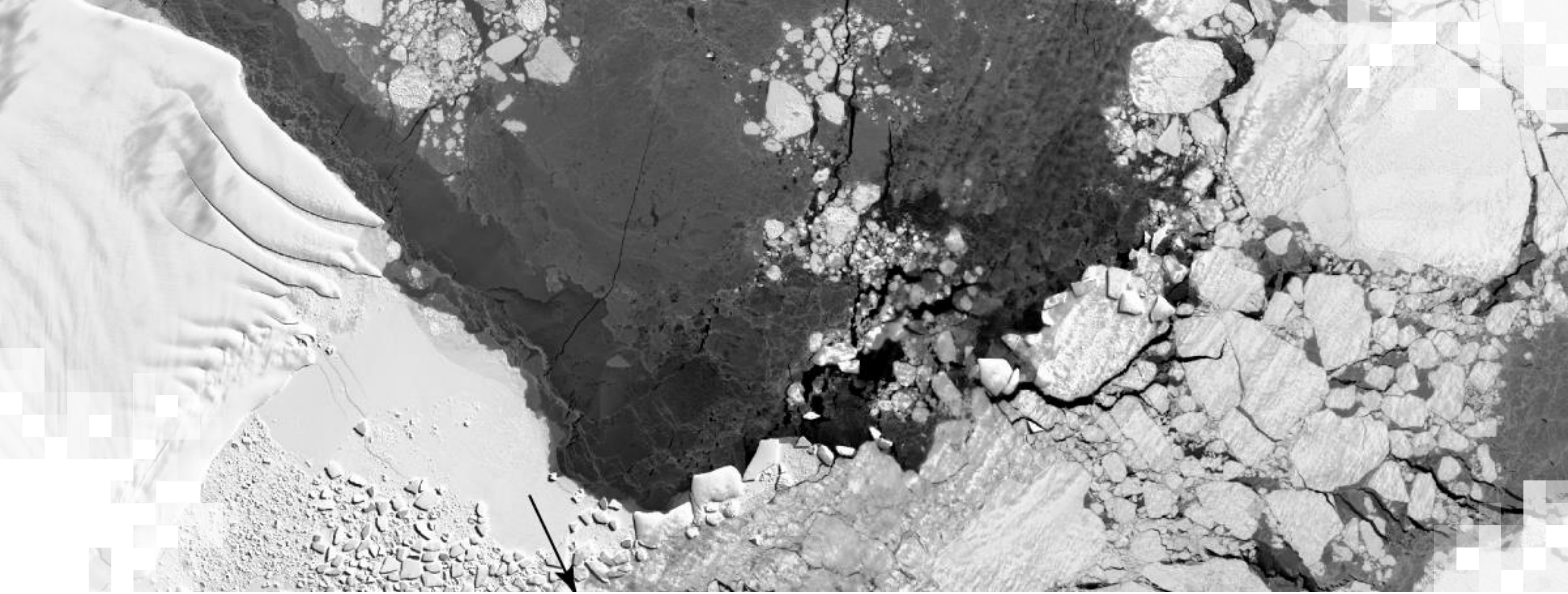

Accessing, Opening, and Displaying SAR Interferometry Time Series Data

Methods – ARIA-tools

- We use pre-processed interferograms from Copernicus Sentinel-1 (S1) satellites that were systematically processed with the ARIA system (Bekaert et al., 2019).
- ARIA Geocoded Unwrapped (GUNW) interferograms are archived at the NASA ASF DAAC.
- You can find the available GUNW files by searching https://search.asf.alaska.edu/#/ and choosing "ARIA S1 GUNW".
- ARIA-tools Package (https://github.com/aria-tools/ARIA-tools) can download and prepare files for time-series analysis.
- ARIA-tools-docs (https://github.com/aria-tools/ARIA-tools-docs) describe usage of ARIA-tools to read the ARIA products.

Methods – MintPy

- After downloading and preparing the ARIA S1 GUNW files (or coregistered interferograms from other processing systems)
- The time-series analysis is done with MintPy (Yunjun et al., 2019) (https://github.com/insarlab/MintPy)
- MintPy Tutorials describe the use of MintPy (https://github.com/insarlab/MintPy-tutorial) for time-series analysis of stacks of interferograms
- MintPy can be installed with Anaconda or Miniconda (conda install mintpy aria-tools)
- See ARIA-tools GitHub for installation methods of ARIA-tools

Data Processing Demonstration

1. The steps of the data processing with ARIA-tools and MintPy are in the Jupyter notebook.

2. This demonstration uses the Alaska SAR Facility (ASF) Open SAR Lab, a cloud-processing system running on AWS.

3. See ASF Open Science Lab (https://opensciencelab.asf.alaska.edu/portal/hub/home) to request an OpenSARLab account. Free for non-commercial use.

Acknowledgments

- Caltech: Z. Yunjun
- JPL: H. Fattahi, D. Bekaert, ARIA Processing Team
- ASF: OpenSARLab Team
- NASA Earth Surface and Interior, Geodetic Imaging, and NISAR Science Team Programs
- California Department of Water Resources

Contact Information

Instructors:

- Instructor
  – Eric.J.Fielding@jpl.nasa.gov
- Subsidence InSAR:
  – Zhen.Liu@jpl.nasa.gov

- ARSET Website
- Follow us on Twitter!
  – @NASAARSET
- ARSET YouTube

Visit our Sister Programs:

- DEVELOP
- SERVIR

APPLIED REMOTE SENSING TRAINING PROGRAM

TRAIN - EMPOWER - ADVANCE

Thank You!